

Article

Drone Path Planning for Bridge Substructure Inspection Considering GNSS Signal Shadowing

Phillip Kim  and Junhee Youn *

Department of Future & Smart Construction Research, Korea Institute of Civil Engineering and Building Technology, Goyang-si 10223, Republic of Korea; ph.doit@gmail.com

* Correspondence: younj@kict.re.kr

† Current address: Department of Educational Facilities & Environments Support, Korea Research Foundation of Local Educational Administration, Seoul 03923, Republic of Korea.

Abstract: Drones are useful tools for performing tasks that are difficult for humans. Thus, they are being increasingly utilized in various fields. In smart construction, a range of methods, including robots and drones, has been proposed to inspect facilities and other similar structures. Global navigation satellite system (GNSS) shadowing can occur when large bridge substructures, which are difficult for humans to access, are inspected using drones because GNSS is a major component in drone operation. This study develops a path planning algorithm to address areas with GNSS shadowing. The operation mode of the drone is classified into waypoint selection based on the photography point algorithm (WPS-PPA) and GNSS non-shadowing area algorithm (WPS-GNSA). Both algorithms are experimentally compared for flight performance in the GNSS shadowing area. A field experiment was conducted by varying the distance between the drone and the bridge substructure and by comparing the success of the flights. In successful flights, the GNSS reception of WPS-GNSA reached 1.4 times that of WPS-PPA. Furthermore, even in failed flights, compared to the WPS-PPA algorithm, the WPS-GNSA algorithm continued flight until the GNSS signal further deteriorated. Accordingly, WPS-GNSA is more favorable than WPS-PPA for inspecting bridge substructures under GNSS signal shadowing.



Academic Editor: Higinio González Jorge

Received: 27 December 2024

Revised: 31 January 2025

Accepted: 7 February 2025

Published: 9 February 2025

Citation: Kim, P.; Youn, J. Drone Path Planning for Bridge Substructure Inspection Considering GNSS Signal Shadowing. *Drones* **2025**, *9*, 124. <https://doi.org/10.3390/drones9020124>

Copyright: © 2025 by the authors. Licensee MDPI, Basel, Switzerland. This article is an open access article distributed under the terms and conditions of the Creative Commons Attribution (CC BY) license (<https://creativecommons.org/licenses/by/4.0/>).

Keywords: autonomous operation; drones; facility inspection; global navigation satellite system (GNSS); GNSS shadowing area

1. Introduction

In recent decades, given the continuous safety problems with infrastructure, governments have established legal measures for the management of various types of infrastructure facilities. In South Korea, the “Special Act on the Safety Control and Maintenance of Establishments” was enacted in 2018 to prevent disasters and enhance public safety by performing safety inspections and maintenance [1]. This act includes procedures and targets for safety inspections, detailed safety measures, and emergency safety inspections. Facilities such as bridges, tunnels, and dams are classified into types 1, 2, and 3 based on the need for management, structural safety, and maintenance technology, and the act outlines the safety inspection and diagnosis procedures for each type. The establishment and amendments to the act significantly increased the number of facilities subject to mandatory management from 1758 in 2016 to 7186 in 2020 [2]. Given this continuous increase in the number of facilities subject to safety management, researchers have conducted various studies to reduce the costs and time required for facility safety management.

Drones and other unmanned vehicles are often utilized in various fields to perform standardized tasks or tasks that are too dangerous for humans, such as working in hazardous areas, including nuclear power plants and disaster sites. For national infrastructure, such as nuclear power plants, scholars have studied emergency response measures [3–6] in addition to surveillance systems [7] and physical security systems [8]. Studies on remote disaster response [9], disaster site data construction [10], disaster site exploration [11–13], and disaster mitigation at construction sites [14] have also been conducted. Moreover, studies have been conducted on the development of drones for use across all public safety fields, including disaster management and firefighting [15–17]. In the safety management of facilities, researchers have focused on the safety inspections of dam facilities based on photographic surveying [18], bridge safety inspections [19], and management of state and public lands [20]. Moreover, industry trends indicate that the use of drones in facility management is expected to grow. The international market size and outlook on drones for facility safety inspections are expected to increase from USD 1.82 million in 2019 to USD 5.17 million in 2025 [21], and the domestic market size is projected to grow from KRW 58 billion in 2019 to KRW 378.2 billion in 2025 [22]. This increasing trend indicates that drones are being widely utilized in facility management and various other fields, and their range of applications is expanding.

Currently, the inspection of facilities using drones faces several limitations. The greatest limitation is related to accessibility to structures, such as offshore structures and transmission towers, which are difficult for humans to access, thereby severely limiting facility inspection through manual control. Methods that enable drones to operate autonomously are being developed to address the limitations of manual control. These autonomous control methods can be divided into those that pre-set the flight path of the drone and input it and those that use a ground control system to receive the current position of the drone in real time and transmit the flight path. Both autonomous operation methods must determine the current location and position of the drone in real time to move to the next destination. Therefore, identifying the exact location and position is an integral aspect of drone operation [23]. Based on the model, the drones can determine their current location and position using the global navigation satellite system (GNSS), such as the United States' GPS, Russia's GLONASS, and the European Union's Galileo. However, the location and position cannot always be accurately determined using GNSS. These inaccuracies can be attributed to structures such as buildings in urban areas, which can cause multipath effects owing to the multiple scattering of electromagnetic signals [23,24]. The estimation error of the location and position based on GNSS presents a major problem for drone operation [25]. Furthermore, GNSS shadowing areas could occur beneath large structures such as bridges, making safe and accurate flight difficult or impossible [26–29]. Consequently, the GNSS-based location estimation results vary from those of simultaneous localization and mapping (SLAM)-based location estimation [29], and the operation of the drone stopped in certain cases [30].

To overcome this limitation, researchers have explored methods for determining the location information using video and light detection and radar (LiDAR) data, which are relatively less affected by the indoor/outdoor status and GNSS shadowing, including methods to address the network problem [31,32]. The location can be estimated using information obtained from image sensors combined with inertial information from the inertial measurement unit [33,34] or by extracting features of unchanging elements to detect relative position, movement, etc. [35,36], serving as research examples to facilitate location determination in areas with GNSS shadowing. Drone systems have also been used in the design and development of infrastructure inspection. Drones equipped with three-dimensional (3D) LiDAR and a mini PC have been developed to perform SLAM during

bridge inspection [23]. The inspection procedure was divided into two processes: pre-flight for acquiring information in 3D space and planning trajectories, and main-flight for inspecting the bridge by flying along the planned trajectory. In this process, the location of the drone was obtained through the newly acquired data and pre-acquired information. The fusion of LiDAR and visual-based SLAM has been proposed to achieve robust localization and 3D mapping for indoor facility inspection [37]. LiDAR-based SLAM has been used to obtain a 3D map of the work area, and visual-based SLAM has been used to estimate the position of a drone. Moreover, planning or avoidance of obstacle algorithms based on the fusion of conventional SLAM and deep learning has been reported [38–42]. The extraction of location information based on image data can be divided into three scenarios: no prior information regarding the area, when information is secured, and when information is being developed [43].

In scenarios where there is no prior information on the area, location information needs to be processed and extracted simultaneously when acquiring the data, which requires the development of new models with computing resources for processing image information on the drone itself. In scenarios where information is secured or constructed, a process of collecting information using image and non-image sensors is required during the securing and construction process. Although image-based and other sensor-based location information generation techniques can enable drone operations in areas with GNSS shadowing, they are limited by the additional costs incurred to develop new models and payloads and for collecting information. Consequently, this study proposes an improved path-planning method to enable the autonomous flight of drones in areas with GNSS shadowing to determine the location and position. The development of these algorithms would enable the utilization of commercial drones for infrastructure inspection.

This study presents two algorithms to inspect the substructure of bridges using drones. The algorithms were tested in actual field settings to compare the bridge inspection success rates, GNSS reception status, etc. The results indicate that the proposed path planning algorithm enables autonomous drone operation without the need to develop new systems and collect prior information using the pre-flight process, even in areas with GNSS shadowing, such as those under bridges. This paper contains four chapters. The first chapter presents the Introduction, which includes a review of previous studies. Section 2 proposes the selection of a target area, a basic system for bridge inspection, algorithm development, and field tests of the algorithm. The results of the test and conclusion are presented in Sections 3 and 4, respectively.

2. Methodologies

2.1. Selection of Target Area, Construction of a 3d Grid System for Bridge Inspection and Process

Selecting the drone model and target areas is necessary to develop and experiment with path planning for use in areas with GNSS shadowing. To this end, this study used DJI's Phantom 4 drone from shenzhen, People's Republic of China. Bukhangang Bridge, located across Namyangju City and Yangpyeong County in Gyeonggi Province, South Korea, was set as the development and experimental target area. Bukhangang Bridge, which opened on 31 May 2023, is a two-way, four-lane main span bridge with a length that exceeds 500 m (length = 1075 m; width = 26.56 m). The height of the bridge is approximately 65 m from the surface of the Bukhan River. Figure 1 displays the photographs of the location and current condition of the bridge.

Upon selecting the target area, a 3D model of the inspection target was developed to efficiently operate the bridge inspection drone. Electronic blueprints of the Bukhangang Bridge are available as it is a newly constructed bridge, and a 3D model was constructed based on these blueprints. The constructed 3D blueprints were used as basic bridge

information to search for the drone flight path and inspect the bridge. Figure 2 presents the results of applying the constructed 3D model to South Korea's Vworld electronic map.

The most crucial aspect in generating the flight path for the autonomous operation of the drone for bridge inspection is ensuring that it can operate without colliding with the bridge. Accordingly, a 3D grid system was applied to the 3D bridge model and the surrounding area, and the interference information with the bridge was constructed. The 3D grid system classifies all areas into aerial, ground, underground, and underwater spaces. The bridge and its adjacent areas are subdivided using a 3D grid system, and the system is used to determine whether there is an overlap with the 3D bridge. In cases where the 3D bridge model and 3D grid overlap, the grid is considered to have obstacles, making it a grid that is unsafe for drone flight. Grids that do not overlap with the 3D bridge model are considered viable for drone path-finding.

Figure 3 shows an example of determining the overlap between the 3D bridge model and its adjacent areas.



Figure 1. Current status of the Bukhangang Bridge: (a) Location [44] and (b) Overview [45].



Figure 2. Three-dimensional (3D) model of the Bukhangang Bridge [46].

The foundational data preparation for bridge inspection using drones was completed by establishing the 3D grid system for bridges. Bridge inspection using drones can be delineated into three primary phases. The first phase involves path planning, wherein the 3D grid system is employed to identify flyable regions in the proximity of the bridge. The flight path is determined either manually or by using the path planning algorithm, which is described later. The second phase involves information acquisition for bridge inspection through flight. In this phase, the drone is operated along the predetermined flight path while acquiring photographic data of the bridge using a camera. The last phase involves leveraging the photographic data for bridge inspection. Artificial intelligence

(AI) technology or conventional computer vision techniques are employed to detect cracks, spalling, and efflorescence across various segments of the bridge, enabling the identification and categorization of damage levels based on the type of deterioration.

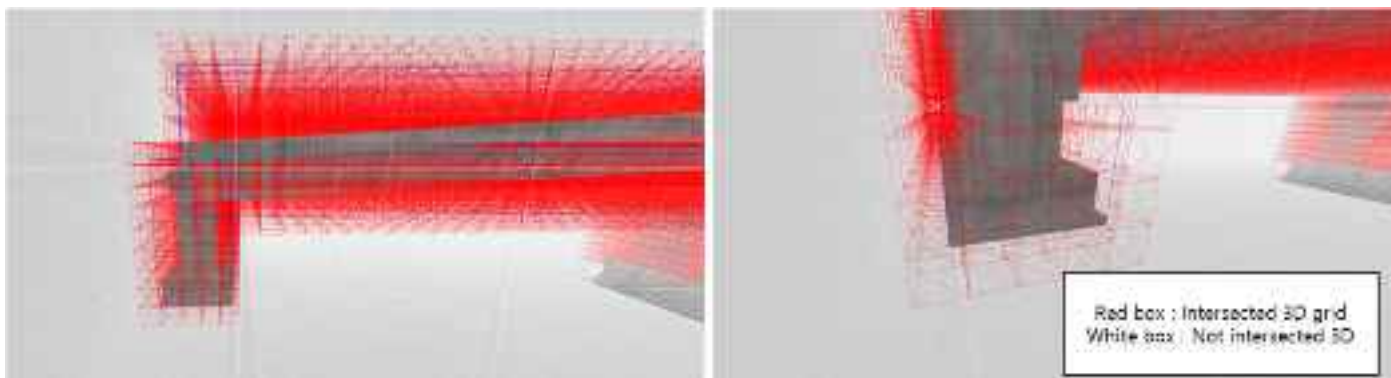


Figure 3. Example for determining 3D grid intersections in the Bukhangang Bridge. The gray, red, and white areas in the figure represent the 3D model of the bridge, grids where flight is impossible due to overlap with the bridge, and grids where flight is possible, respectively.

2.2. Waypoint Selection Based on Photography Point Algorithm

Waypoint selection based on a photography point algorithm (WPS-PPA) that enables efficient flight path setting for bridge inspection was developed. The WPS-PPA aims to set an autonomous flight path for bridge inspection; therefore, it is crucial to ensure that no bridge information is omitted throughout the flight. Bridge information is collected using the drone camera, and the field of view (FOV) is calculated to ensure that spatial image information is not omitted. The FOV is calculated using:

$$FOV = \frac{Sensor\ Size \times Working\ distance}{Focal\ length}. \quad (1)$$

Figure 4 depicts a conceptual diagram of the camera FOV. The working distance, dw , represents the distance from the target object to the lens, while the focal length, f , indicates the distance between the lens and sensor. The FOV is divided into longitudinal, transverse, and diagonal components, with light rays traveling at different angles, α , β , θ , through the lens. The sensor dimensions, w_{sensor} and h_{sensor} , correspond to the captured FOV, illustrating the mapping of the angular coverage of the scene onto the sensor area. The underside of the bridge, a typical area with GNSS shadowing, was selected as the inspection target to test autonomous drone operation in areas with GNSS shadowing during bridge inspection, and an algorithm was proposed to set the flight path for this area. The underside of the bridge can be considered the largest area among the bridge inspection targets (underside, sides, and piers).

The basic spatial information of the bridge can be understood by determining whether each grid intersects with the bridge. The overlap between the bridge and the grids for the entire bridge was derived and utilized in the first step of WPS-PPA.

Subsequently, planar grids that correspond to the underside of the bridge were extracted as the inspection target, and grids that did not intersect with the bridge were considered viable for use in WPS-PPA. A flight path was then determined by combining the FOV equation of the drone and the grids, setting detours around the obstacle areas. Figure 5 illustrates the process as a simple flowchart. The white boxes are grids of the bridge, and the orange boxes are example of flight path.

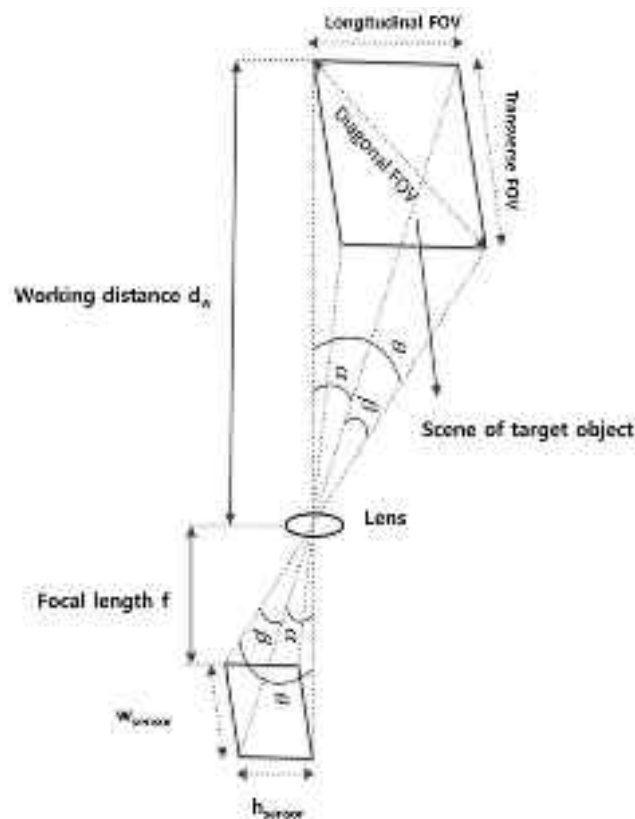


Figure 4. Conceptual diagram of calculating camera FOV [47].

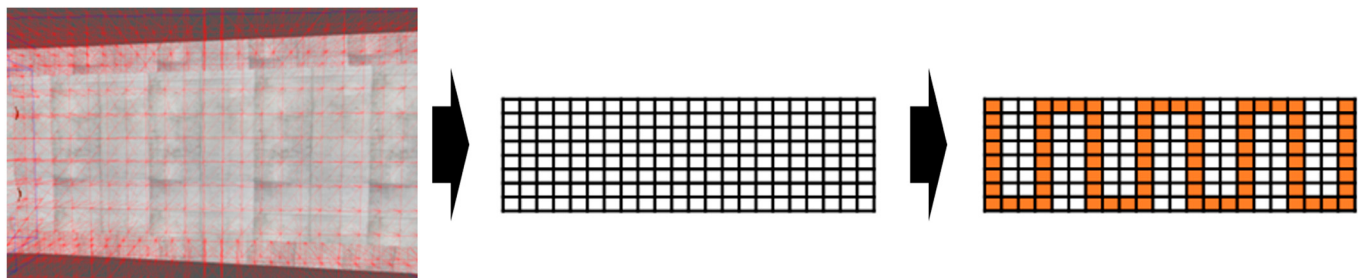


Figure 5. Flowchart for drone path planning.

The method for combining the FOV equation with the grids is as follows:

The 3D grid in which the waypoint for the flight path of the drone is located is defined as:

$$C_{i,j,k} = [C_i, C_j, C_k], \quad (2)$$

where i indicates the number of grid units progressing in the transverse direction of the bridge, j indicates the number of grid units progressing in the longitudinal direction of the bridge, and k indicates the number of grid units progressing in the vertical direction from the bridge to the ground surface.

The grid from which the starting point for the drone flight is located is defined as $C_{0,0,0}$. The distance of movement in each direction of i , j , and k needs to be determined to move from the starting point to the next point. For the k direction, the flight path is set for inspecting the underside of the bridge, and therefore, it remains fixed at the initially set value. The flight altitude of the drone is set to remain the same, determined by the height of the bridge and the operating distance of the drone. C_k is determined using:

$$C_k = H - D_w, \quad (3)$$

where H and D_w represent the height of the bridge and the working distance, respectively. Additionally, the progression in the transverse direction to the bridge is also determined. The transverse movement distance after one shooting session must be determined for transverse progression. This was set to ensure zero overlap in the images obtained during the bridge inspection process. Therefore, the transverse movement was set to proceed with the transverse FOV of the image shot by the drone, which is FOV_t . If an overlap in the transverse shooting is required based on the case, the movement distance can be adjusted to $(1 - \text{Transverse Duplication}) \times FOV_t$ for the operation. The change in $C_{i,j,k}$ attributed to the transverse movement can be expressed using:

$$C_i = C_{i-1} + FOV_t, C_{i,j,k} = [C_{i-1} + FOV_t, C_{j-1}, C_{k-1}], \quad (4)$$

where FOV_t represents the length of the transverse FOV.

The longitudinal movement was performed after reaching the opposite end of the underside of the bridge through transverse movement and acquiring all images that correspond to C_i . Similar to the transverse movement, the longitudinal movement was set to have no overlap in the longitudinal direction and proceed by the longitudinal FOV of the image, which is FOV_l . If the overlap in the longitudinal shooting is required based on the case, the movement distance can be adjusted to $(1 - \text{Longitudinal Duplication}) \times FOV_l$ for operation. The change in $C_{i,j,k}$ attributed to the longitudinal movement can be expressed by

$$C_j = C_{j-1} + FOV_l, C_{i,j,k} = [C_{i-1}, C_{j-1} + FOV_l, C_{k-1}], \quad (5)$$

where FOV_l represents the longitudinal length of the FOV. Upon moving once longitudinally, the transverse movement was repeated, completing the entire process of bridge inspection by acquiring image data from the entire underside area of the bridge using the drone, as shown in Figure 6. During the flight, the drone moves by setting each waypoint as the destination point. Figure 7 presents the actual results of setting the drone flight path based on WPS-PPA.

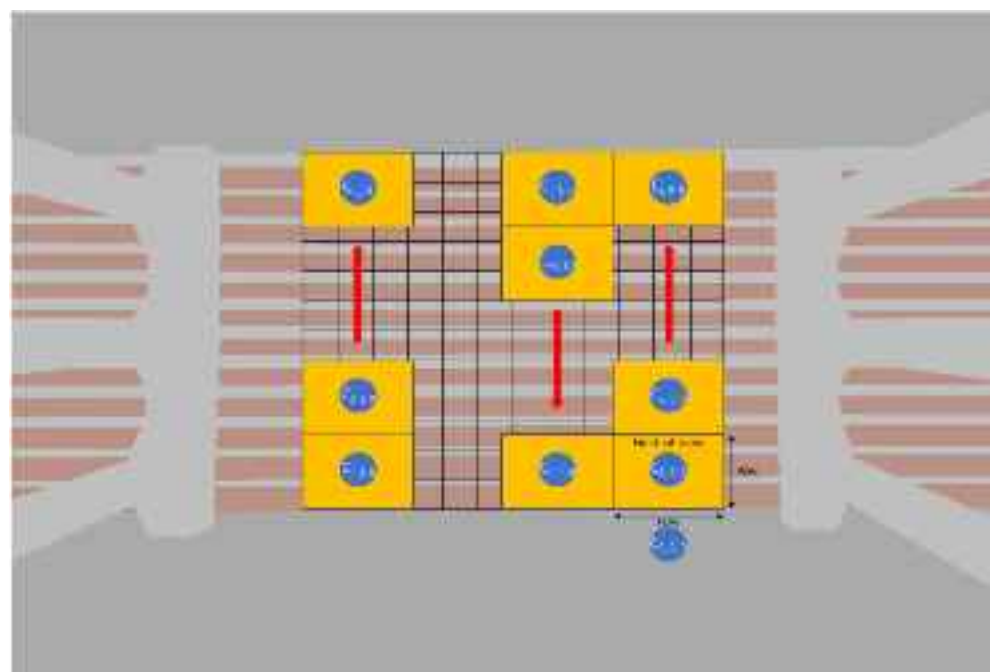


Figure 6. Conceptual diagram of the drone flight path based on WPS-PPA. The yellow surface represents the FOV of the drone, the blue dots represent the set waypoints, the black grids are examples of the 3D grid system, and the red arrows are direction of drone.



Figure 7. Results of setting drone flight path based on WPS-PPA. The gray points represent the waypoints, blue line represents the flight path, and the yellow lines represent the FOV of the drone.

The WPS-PPA for bridge inspection is considered an efficient method that can minimize the distance traveled under the bridge, thereby enabling efficient acquisition of image data of the inspection target facilities through drone operation.

2.3. Waypoint Selection Based on GNSS Non-Shadowing Area Algorithm

Despite its efficiency, WPS-PPA operates without leaving the underside of the bridge and sets each point where the image is shot as a waypoint, causing the operation to stop when these points are in areas with GNSS shadowing. Therefore, an additional waypoint selection based on the GNSS non-shadowing area algorithm (WPS-GNSA), which does not place waypoints in the areas with GNSS shadowing under the bridge, was developed; each waypoint is located only outside the bridge. The WPS-GNSA was developed with the following two objectives:

1. Not to fly only under the bridge but to move the shortest distance from outside the bridge to outside on the opposite side, placing waypoints only outside the bridge and minimizing the time spent under the bridge.
2. Performing tasks automatically based on time or distance instead of setting waypoints and assigning tasks at each point during the drone mission assignment process.

Similar to the WPS-PPA, the relationship between the bridge and the location of the drone was utilized to fly the shortest distance under the bridge by combining the FOV equation and the grid. Similarly, the 3D grid where the waypoint for the flight path of the drone is located was defined as $C_{i,j,k}$ according to Equation (2), and the starting point of the drone is defined as $C_{0,0,0}$. In WPS-GNSA, the starting point of the drone was determined considering FOV_t and FOV_l for more efficient drone operation. Compared to the outermost point of the bridge, the point moving $FOV_t/2$ in the i direction and $FOV_l/2$ in the j direction becomes $C_{0,0,0}$. Similar to WPS-PPA, after moving in the i direction, it was decided to move once in the j direction, and the k direction was fixed as in Equation (3).

In WPS-GNSA, the transverse movement was determined to start from one outside edge and move to the opposite outside edge. Therefore, moving in the i direction transverse to the bridge, the movement was set to the length of the bridge plus FOV_t , moving to the same position on the opposite side. This can be expressed as

$$\begin{aligned} C_i &= C_{i-1} + BL_V + FOV_t, \\ C_{i,j,k} &= [C_{i-1} + BL_t + FOV_l, C_{j-1}, C_{k-1}], \end{aligned} \quad (6)$$

where BL_v and FOV_t represent the transverse length of the bridge and the transverse length of the FOV, respectively. In the transverse movement process, WPS-GNSA was set to acquire image information based on pre-determined time or distance intervals, unlike the WPS-PPA, which acquired image information at each waypoint using the camera.

Upon completing one transverse movement, the longitudinal movement, which is parallel to the bridge, was set to be the same as Equation (5), similar to WPS-PPA. The entire bridge inspection process using drones was completed by acquiring image data of the entire underside area of the bridge by repeating this process, as shown in Figure 8. During the flight, the drone moves by setting each waypoint as the destination point. The actual results of setting the drone flight path based on WPS-GNSA are shown in Figure 9.

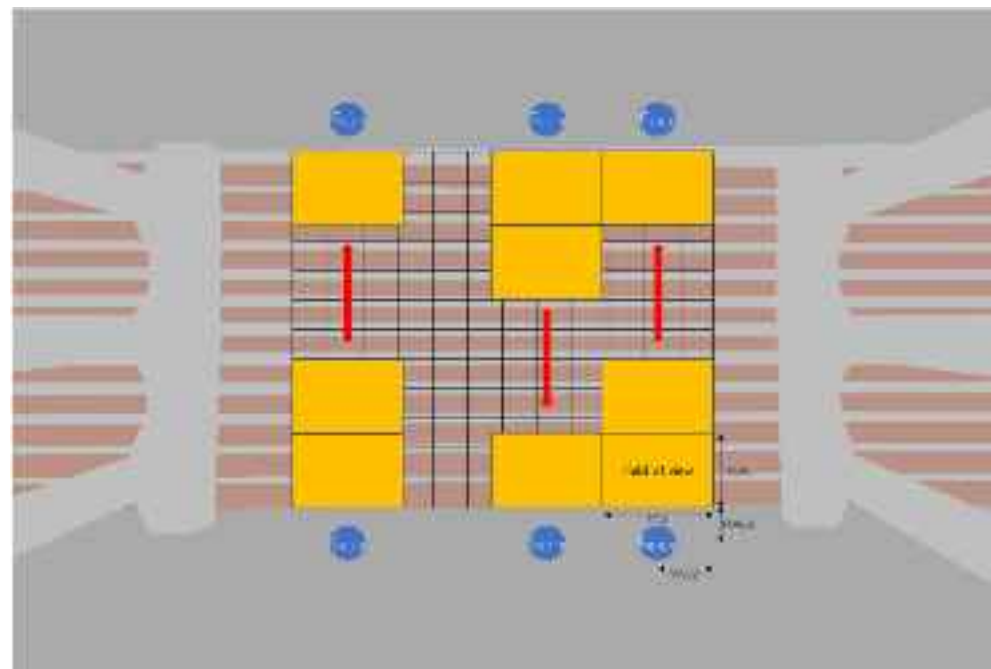


Figure 8. Conceptual diagram of the drone flight path based on WPS-GNSA. The yellow surface represents the drone's FOV, the blue dots represent the set waypoints, the black grids are examples of the 3D grid system, and the red arrows are direction of drone.



Figure 9. Results of setting the drone flight path based on WPS-GNSA. The gray points represent the waypoints, blue line represents the flight path, and the yellow lines represent the drone's FOV.

As shown in Figures 7 and 9, WPS-PPA and WPS-GNSA each set waypoints based on their respective methods, and it is evident that the number of waypoints differs markedly even along the same path.

2.4. Field Experiment Method

Field experiments were conducted to examine the drone operation in areas with GNSS shadowing and evaluate the usability of WPS-PPA and WPS-GNSA in the actual bridge inspection environment. The field experiment involved varying the separation distance between the underside of the bridge deck and the drone. Table 1 summarizes the field experiment, and Figure 10 presents the view from under the bridge and the situation of the field experiment. The red box shown in Figure 10b depicts the drone during actual operation.

- (1) Successful drone flight: The drone was flown according to a pre-set flight path, and the success of the flight was compared for each algorithm, regardless of the areas with GNSS shadowing.
- (2) Comparison of GNSS levels provided by the drone manufacturer: DJI drones provide a GNSS level based on a comprehensive judgment of GNSS reception status, number, etc., and the GNSS level of flights using each algorithm was compared. Table 2 presents the GNSS-level classifications provided by DJI and the explanations for each category.
- (3) Number of GNSS connections: DJI drones provide the number of connected GNSS along with the GNSS level at 0.5-s intervals during flight. The average number of connections for each level was compared based on the GNSS level mentioned earlier. However, we presented the proportion of each level and the number of connections during the entire flight because the number of GNSS level data collected varies with the total flight time.

Table 1. Summary of the field experiments.

Date	5 October 2023
Target of field experiment	Bukhangang Bridge (Namyangju City, Rep. of Korea)
Model of drone	Phantom 4 (DJI)
Test algorithm	WPS-GNSA WPS-PPA

Table 2. GPS levels for DJI drones and explanation [48].

Level	Description
0	The GPS has almost no signal, which is very bad.
1	The GPS signal is very weak.
2	The GPS signal is weak. At this level, the drone's go-home functionality will still work.
3	The GPS signal is good. At this level, the drone can hover in the air.
4	The GPS signal is very good. At this level, the drone can record the home point.
5	The GPS signal is very good.
None	There is no GPS signal



Figure 10. Field experiment status of the Bukhangang Bridge: (a) Underneath and (b) Drone operation, and the red box shows the drone.

3. Results & Discussion

Experiments were conducted by varying the separation distance between the underside of the bridge deck and the drone. The closer the separation distance between the bridge deck and the drone, the farther the distance from the ground surface; further, the range of areas with GNSS shadowing also expanded. The results are presented in Table 3.

Table 3. Experimental Results.

Algorithm	Separation Distance [m]	Success/Failure (Flight Duration [s])	GNSS Level Ratio	Number of GNSS Connections (Min–Max)
WPS-PPA	15	Failure (32)	Level 4	71.9% 11.9 (9–14)
			Level 3	28.1% 6.8 (6–7)
	19	Success (124)	Level 4 Level 3	60.5% 39.5% 9.8 (8–13) 7.6 (6–10)
WPS-GNSA	23	Failure (18)	Level 4	100.0% 9.5 (8–11)
	17	Failure (27)	Level 5	40.7% 15.2 (14–16)
			Level 4	48.1% 13.0 (10–15)
			Level 3	11.2% 7.0 (6–8)
	19	Success (138)	Level 5	9.4% 15.2 (14–16)
			Level 4	70.3% 12.2 (8–16)
			Level 3	20.3% 8.6 (6–13)
	23	Failure (21)	Level 4 Level 3	81.0% 19.0% 10.7 (9–12) 8.3 (7–9)

The success of flight refers to a scenario in which the drone completed its flight according to the given path plan without any problems. Failure refers to the scenario in which the drone is unable to complete the flight as planned owing to interrupted operation. From the perspective of flight mission success, flights failed except when the separation distance was 19 m from the top. GNSS shadowing and the geometric shape of the area are expected to be most influenced by the distance from the bridge, but other factors, such as the position of satellites over time, will also play a role. The failure when the separation

distance was increased to 23 m, despite the expectation that the areas with GNSS shadowing decrease compared to that with the original 19 m, indicates that the success of the drone's flight is not solely determined by the distance from the bridge. Since the drone's continuous flight maintenance depends not only on GNSS but also on the accurate determination of its position, orientation, and direction through various sensor data, a comprehensive analysis considering the differences between drone models and scenarios is necessary.

For both algorithms with the same separation distance of 19 m, WPS-PPA only showed GNSS levels 4 and 3. WPS-GNSA also showed GNSS level 5. Although the proportion of GNSS level 4 for WPS-PPA was 60.5%, the proportion of GNSS level 4 and above for WPS-GNSA was 79.7%, indicating better reception conditions. In addition, the number of GNSS connections for each level was also higher in WPS-GNSA.

For cases of failed flights under the same separation distance of 23 m, WPS-PPA showed better GNSS reception conditions with 100% GNSS level 4 compared to WPS-GNSA. However, this was a case of flight failure, suggesting that WPS-PPA failed before reaching GNSS level 3, while WPS-GNSA, despite failing, managed to fly for a short duration even after entering GNSS level 3.

An additional analysis of the number of observable GNSS at the site during the experimental period was conducted. It was confirmed that 15 to 17 GNSS (GPS and GLONASS) were consistently observed throughout the experimental period. This demonstrates that each experiment was conducted under similar conditions and shows that WPS-GNSA achieved better flight results compared with WPS-PPA under these comparable conditions.

4. Conclusions

This study aimed to develop flight algorithms to improve the efficiency of drone operation in areas with GNSS shadowing that can occur during bridge inspection using drones. A 3D grid system was constructed around the bridge area, and WPS-PPA was developed, placing all paths in the grid to set the drone's flight path. Moreover, WPS-GNSA was developed to minimize the time spent by the drone under the bridge by setting the departure and arrival points outside rather than under the bridge and only using these points as waypoints. Large structures such as bridges can disrupt GNSS signal reception even without being fully enclosed, resulting in the formation of GNSS shadow areas. Consequently, these shadow areas may hinder the accurate estimation of position and location during inspections using drones.

The results of the experiments conducted on Bukhangang Bridge showed that in successful flight cases, WPS-GNSA had a higher GNSS level and number of connections than WPS-PPA, indicating better reception conditions. Even in cases of flight failure, the operation was deemed possible until the GNSS reception conditions worsened; hence, WPS-GNSA was found to be more advantageous for inspecting the bottom structure of bridges compared to WPS-PPA. The WPS-GNSA algorithm enabled flights in the GNSS-shadowed areas beneath bridges, demonstrating the feasibility of using drones for bridge inspection.

Various methods beyond the path planning algorithms were proposed in previous studies to perform bridge inspection in the GNSS-shadowed areas. The state-of-the-art approaches applicable to bridge detection include real-time location determination using sensors such as LiDAR, which then serve as the basis for path planning. However, these studies often involved modifying the existing drones to develop new features or creating new H/W systems specifically for facility inspection. The results of this study demonstrate that flight in GNSS-shadowed areas can be achieved by developing a path-planning algorithm without the need for new H/W systems or features. This enables the inspection of bridge substructures using commercially available drones, which is highly advantageous. The algorithm could further be enhanced to incorporate collision avoidance with moving

obstacles during the inspection of bridge substructures and to implement these improvements in real-time using onboard computing, thereby increasing the practical applicability of the algorithm.

Despite the increase in the distance from the bridge deck, the successes of flight occasionally turned into failures or vice versa. Increasing the distance from the bridge deck can theoretically reduce the areas with GNSS shadowing; however, the field experiment results do not imply that the success rate of flight can be increased by simply increasing the distance from the bridge. Despite the reduction in the GNSS shadowing areas caused by the bridge deck with the increase in distance, other factors can still affect GNSS reception. The factors that affect GNSS reception outside. Each test flight could not be conducted simultaneously at the same location; it was conducted sequentially. This caused variations in the different factors; moreover, changes in the number of satellites available for reception based on the time of day also contributed to the variations. The success of the flight depends on various factors, including the distance from the bridge deck, weather, and time of day. Therefore, additional flight experiments under various cases using the two proposed algorithms will provide more detailed comparisons of their accuracy. Furthermore, additional experiments must be conducted on bridges located in different areas with varying geographical features or characteristics and bridge forms, as well as on various drone models, to comprehensively test the applicability of the algorithms and improve their generalizability.

Author Contributions: Conceptualization, P.K. and J.Y.; methodology, P.K.; validation, P.K. and J.Y.; formal analysis, P.K.; investigation, J.Y.; resources, J.Y.; data curation, P.K.; writing—original draft preparation, P.K.; writing—review and editing, J.Y.; visualization, P.K.; supervision, J.Y.; project administration, J.Y.; funding acquisition, J.Y. All authors have read and agreed to the published version of the manuscript.

Funding: This research was funded by the Korea Agency for Infrastructure Technology Advancement grant funded by the Ministry of Land, Infrastructure, and Transport (Grant No. RS-2022-00143782, Development of Fixed/Moving Platform Based Dynamic Thematic Map Generation Technology for Next Generation Digital Land Information Construction).

Data Availability Statement: The data presented in this study are available on request from the corresponding author due to legal reasons.

Conflicts of Interest: The authors declare no conflicts of interest.

References

1. Ministry of Land, Infrastructure and Transport, Republic of Korea. *Special Act on the Safety Control and Maintenance of Establishments*; Ministry of Land, Infrastructure and Transport, Republic of Korea: Sejong, Republic of Korea, 2017.
2. Park, J.; Kim, S.G. *Structural Safety Management for Small-Scale Buildings*; The Seoul Institute: Seoul, Republic of Korea, 2019.
3. Park, J.; Choi, Y.S. An aerial and ground monitoring system for nuclear accidents. In Proceedings of the Transactions of the Korean Nuclear Society Spring Meeting, Jeju, Republic of Korea, 18–19 May 2017.
4. Lee, S.U.; Choi, Y.; Jeong, K. Domestic recent works on robotic system for safety of nuclear power plants. *J. Korean Soc. Precis. Eng.* **2019**, *36*, 323–329. [[CrossRef](#)]
5. Hussain, M.; Mehboob, K.; Ilyas, S.Z.; Shaheen, S.; Abdulsalam, A. Drones application scenarios in a nuclear or radiological emergency. *Kerntechnik* **2022**, *87*, 260–270. [[CrossRef](#)]
6. Sato, Y.; Ozawa, S.; Terasaka, Y.; Minemoto, K.; Tamura, S.; Shingu, K.; Nemoto, M.; Torii, T. Remote detection of radioactive hotspot using a Compton camera mounted on a moving multi-copter drone above a contaminated area in Fukushima. *J. Nucl. Sci. Technol.* **2020**, *57*, 734–744. [[CrossRef](#)]
7. Seo, J.W.; Han, S.H.; Park, J.H.; Shin, S. Nuclear power plant monitoring system using drone. In Proceedings of the Summer Conference, Virtual, 13–16 September 2020; The Korean Institute of Communications and Information Sciences: Seoul, Republic of Korea, 2020; pp. 909–910. Available online: <https://journal-home.s3.ap-northeast-2.amazonaws.com/site/2020kics/presentation/0675.pdf> (accessed on 31 January 2025).

8. Choi, Y.J.; Kim, J.S. A study on the utilization of drones and the improvement plan of physical security of nuclear power plants. *Korean Secur. J.* **2022**, *70*, 195–216.
9. Park, N.; Ahn, Y.; Hwang, Y. A study on the development of a remote control drone for disaster response. *J. Korean Soc. Disaster Inf.* **2019**, *15*, 578–589.
10. Pi, Y.; Nath, N.D.; Behzadan, A.H. Convolutional neural networks for object detection in aerial imagery for disaster response and recovery. *Adv. Eng. Inf.* **2020**, *43*, 101009. [CrossRef]
11. Nam, K.H.; Jang, M.S. A study on the exploration device of the disaster site using drones. *J. Korean Inst. Electron. Commun. Sci.* **2019**, *14*, 579–586.
12. Kyrikou, C.; Plastiras, G.; Theocharides, T.; Venieris, S.I.; Bouganis, C.S. DroNet: Efficient convolutional neural network detector for real-time UAV applications. In Proceedings of the 2018 Design, Automation & Test in Europe Conference & Exhibition, Dresden, Germany, 19–23 March 2018; pp. 967–972.
13. Lygouras, E.; Santavas, N.; Taitzoglou, A.; Tarchanidis, K.; Mitropoulos, A.; Gasteratos, A. Unsupervised human detection with an embedded vision system on a fully autonomous UAV for search and rescue operations. *Sensors* **2019**, *19*, 3542. [CrossRef]
14. Lim, B.J.; Park, J.Y. A study on reducing construction site disasters through the use of drones. *J. Disaster Saf.* **2020**, *29*–39.
15. Ju, H.J.; Lim, K.S.; Kim, H.J. The develop necessity of the multifunctional drones against cope with various disasters. *Korean J. Sci. Crim. Investig.* **2023**, *17*, 186–195.
16. Kim, B.; Kim, J. A study on the efficient operation of drones in public safety. *J. Hum. Soc. Sci.* **2022**, *13*, 1827–1836.
17. Ha, K.H.; Kim, J.H.; Choi, J.W. A study on the application of drone in firefight field. *J. Korean Acad. Ind. Coop. Soc.* **2021**, *22*, 321–330.
18. Park, D.S.; Yu, J.I.; You, H. A research on applicability of drone photogrammetry for dam safety inspection. *J. Korean Inst. Struct. Maint. Insp.* **2023**, *27*, 30–39.
19. Lee, S.B.; Lee, K.; Choi, H.M.; Lim, C.S. Establishment of a standard procedure for safety inspections of bridges using drones. *KSCE J. Civ. Environ. Eng. Res.* **2022**, *42*, 281–290.
20. Lih, B.J.; Koh, J.H. A study on construction plan of the national & public land management model based on the drone. *J. Korean Soc. Cadastre* **2016**, *32*, 85–102.
21. *Drone Surveillance Market for Energy & Power*; Fortune Business Insights: Pune, India, 2020.
22. Drone for Infrastructure Safety Inspection. Available online: https://tb.kibo.or.kr/ktbs/board/tech-trend/tech_trend.do?mode=view&articleNo=481&article.offset=0&articleLimit=10&srSearchVal=%EC%8B%9C%EC%84%A4%EB%AC%BC&srSearchKey=article_title (accessed on 24 January 2024).
23. Liu, Y.; Bai, J.; Wang, G.; Wu, X.; Sun, F.; Guo, Z.; Geng, H. UAV localization in low-altitude GNSS-denied environments based on poi and store signage text matching in UAV images. *Drones* **2023**, *7*, 451. [CrossRef]
24. Jiang, Z.; Groves, P.D. NLOS GPS signal detection using a dual-polarisation antenna. *GPS Solut.* **2014**, *18*, 15–26. [CrossRef]
25. Mandirola, M.; Casarotti, C.; Peloso, S.; Lanese, I.; Brunesi, E.; Senaldi, I. Use of UAS for damage inspection and assessment of bridge infrastructures. *Int. J. Disaster Risk Reduct.* **2022**, *72*, 102824. [CrossRef]
26. Duque, L. UAV-Based Bridge Inspection and Computational Simulations. Master’s Thesis, South Dakota State University, Brookings, SD, USA, 2017.
27. Morgenthal, G.; Hallermann, N.; Kersten, J.; Taraben, J.; Debus, P.; Helmrich, M.; Rodehorst, V. Framework for automated UAS-based structural condition assessment of bridges. *Autom. Constr.* **2019**, *97*, 77–95. [CrossRef]
28. Ali, R.; Kang, D.; Suh, G.; Cha, Y.J. Real-time multiple damage mapping using autonomous UAV and deep faster region-based neural networks for GPS-denied structures. *Autom. Constr.* **2021**, *130*, 103831. [CrossRef]
29. Kim, I.H.; Yoon, S.; Lee, J.H.; Jung, S.; Cho, S.; Jung, H.J. A comparative study of bridge inspection and condition assessment between manpower and a UAS. *Drones* **2022**, *6*, 355. [CrossRef]
30. Araar, O.; Aouf, N. A new hybrid approach for the visual servoing of VTOL UAVs from unknown geometries. In Proceedings of the 22nd Mediterranean Conference on Control and Automation, Palermo, Italy, 16–19 June 2014; pp. 1425–1432.
31. Li, W.; Shi, M.; Shi, L.; Lin, B.; Qin, K. Containment tracking for networked agents subject to nonuniform communication delays. *IEEE Trans Netw. Sci. Eng.* **2023**, *10*, 3658–3669. [CrossRef]
32. Li, W.; Qin, K.; Li, G.; Shi, M.; Zhang, X. Robust bipartite tracking consensus of multi-agent systems via neural network combined with extended high-gain observer. *ISA Trans.* **2023**, *136*, 31–45. [CrossRef]
33. Diel, D.D.; DeBitetto, P.; Teller, S. Epipolar constraints for vision-aided inertial navigation. In Proceedings of the 2005 7th IEEE Workshops on Applications of Computer Vision (WACV/MOTION’05)-Volume 1, Breckenridge, CO, USA, 5–7 January 2005; pp. 221–228.
34. Wen, H.; Tian, J.; Li, D. PLS-VIO: Stereo vision-inertial odometry based on point and line features. In Proceedings of the 2020 International Conference on High Performance Big Data and Intelligent Systems (HPBD&IS), Shenzhen, China, 23 May 2020; pp. 1–7.

35. Cho, D.M.; Tsiotras, P.; Zhang, G.; Holzinger, M. Robust feature detection, acquisition, and tracking for relative navigation in space with a known target. In Proceedings of the AIAA Guidance, Navigation, and Control (GNC) Conference, Boston, MA, USA, 19–22 August 2013. AIAA 2013-5197.
36. Szenher, M.D. Visual homing in dynamic indoor environments. In Proceedings of the 13th IASTED International Conference on Robotics and Applications, Würzburg, Germany, 29–31 August 2008.
37. Gao, C.; Wang, X.; Wang, R.; Zhao, Z.; Zhai, Y.; Chen, X.; Chen, B.M. A UAV-based explore-then-exploit system for autonomous indoor facility inspection and scene reconstruction. *Autom. Constr.* **2023**, *148*, 104753. [[CrossRef](#)]
38. Michels, J.; Saxena, A.; Ng, A.G. High speed obstacle avoidance using monocular vision and reinforcement learning. In Proceedings of the 22nd International Conference on Machine Learning, Bonn, Germany, 7–11 August 2005; pp. 593–600.
39. Vamvoudakis, K.G.; Vrabie, D.; Lewis, F.L. Online adaptive algorithm for optimal control with integral reinforcement learning. *Int. J. Robust Nonlinear Control* **2014**, *24*, 2686–2710. [[CrossRef](#)]
40. Kulkarni, T.D.; Narasimhan, K.; Saeedi, A.; Tenenbaum, J. Hierarchical deep reinforcement learning: Integrating temporal abstraction and intrinsic motivation. *Adv. Neural Inform. Process. Syst.* **2016**, *29*, 3682–3690.
41. Xie, L.; Wang, S.; Markham, A.; Trigoni, N. Towards monocular vision based obstacle avoidance through deep reinforcement learning. *arXiv* **2017**, arXiv:1706.09829.
42. Xu, Y.; Wei, Y.; Wang, D.; Jiang, K.; Deng, H. Multi-UAV Path Planning in GPS and Communication Denial Environment. *Sensors* **2023**, *23*, 2997. [[CrossRef](#)] [[PubMed](#)]
43. Lu, Y.; Xue, Z.; Xia, G.S.; Zhang, L. A survey on vision-based UAV navigation. *Geo-Spat. Inf. Sci.* **2018**, *21*, 21–32. [[CrossRef](#)]
44. Naver Map. Available online: <https://map.naver.com> (accessed on 27 March 2024).
45. Joongang.tv. Available online: <http://www.joongang.tv/news/articleView.html?idxno=64579> (accessed on 24 January 2024).
46. Vworld. Available online: <https://www.vworld.kr> (accessed on 27 March 2024).
47. VisionTIR. Available online: <https://visiontir.com/7-factors-when-choosing-a-thermal-camera-for-temperature-measurement/> (accessed on 24 January 2024).
48. DJI Android Mobile SDK Reference. Available online: <https://developer.dji.com/iframe/mobile-sdk-doc/android/reference/dji/common/flightcontroller/DJIGPSSignalStatus.html> (accessed on 24 January 2024).

Disclaimer/Publisher’s Note: The statements, opinions and data contained in all publications are solely those of the individual author(s) and contributor(s) and not of MDPI and/or the editor(s). MDPI and/or the editor(s) disclaim responsibility for any injury to people or property resulting from any ideas, methods, instructions or products referred to in the content.